An Experimental Evaluation of Generalized Predictive Control for Tiltrotor Aeroelastic Stability Augmentation in Airplane Mode of Flight

Raymond G. Kvaternik and David J. Piatak
NASA Langley Research Center
Hampton, Virginia

Mark W. Nixon, Chester W. Langston, and Jeffrey D. Singleton
Army Research Laboratory
Vehicle Technology Directorate
NASA Langley Research Center
Hampton, Virginia

Richard L. Bennett and Ross K. Brown
Bell Helicopter Textron
Fort Worth, Texas

The results of a joint NASA/Army/Bell Helicopter Textron wind-tunnel test to assess the potential of Generalized Predictive Control (GPC) for actively controlling the swashplate of tiltrotor aircraft to enhance aeroelastic stability in the airplane mode of flight are presented. GPC is an adaptive time-domain predictive control method that uses a linear difference equation to describe the input-output relationship of the system and to design the controller. The test was conducted in the Langley Transonic Dynamics Tunnel using an unpowered 1/5-scale semispan aeroelastic model of the V-22 that was modified to incorporate a GPC-based multi-input multi-output control algorithm to individually control each of the three swashplate actuators. Wing responses were used for feedback. The GPC-based control system was highly effective in increasing the stability of the critical wing mode for all of the conditions tested, without measurable degradation of the damping in the other modes. The algorithm was also robust with respect to its performance in adjusting to rapid changes in both the rotor speed and the tunnel airspeed.

Notation

$\mathcal{A}, \mathcal{B}, \mathcal{T}$	matrices (formed from α_i and β_i) in multi-step output prediction equation
h_c	control horizon
h_p	prediction horizon
J	objective function to be minimized
k	time index
l	number of data time steps used for SID
m	number of feedback outputs to GPC
p	order of ARX equation describing system
Q, R	weighting matrices for inputs and outputs
r	number of control inputs from GPC
$u(k)$	vector of digitized input time histories
u_c	vector of computed control inputs
V	matrix of input and output measurements
w_c, w_r	weighting factors for inputs and outputs
$\overline{Y}$	matrix of OMP determined by SID
$y(k)$	vector of digitized response time histories
α^c, β^c	control law gain matrices
α_i, β_i	coefficient matrices (OMP) appearing in ARX equation and determined by SID
δ_3	blade kinematic pitch-flap coupling angle
ε	error function (difference between target and predicted responses)

Abbreviations:

ARX	autoregressive with exogenous input
MIMO	multi-input/multi-output
OMP	observer Markov parameters
SID	system identification

INTRODUCTION

Tiltrotor aircraft operating at high speeds in the airplane mode of flight are susceptible to a proprotor/pylon instability akin to propeller whirl flutter. Such an instability was first encountered during full-scale testing of the Bell XV-3 tiltrotor in the NASA-Ames 40- by 80-foot Wind Tunnel in 1962. Following this incident, extensive analytical and experimental studies of small dynamically-scaled models were initiated by Bell with the threefold objective of providing a physical understanding of the phenomenon, developing an analytical method to predict such instabilities, and identify-

Presented at the American Helicopter Society 57th Annual Forum, Washington, DC, May 9-11, 2001.

ing corrective design changes. By 1965, both an explanation for and a means for eliminating the instability were found (refs. 1-2). The XV-3 aircraft was then modified to incorporate changes indicated by analyses and retested successfully in the NASA-Ames 40- by 80-foot Wind Tunnel in 1966. The proprotor/pylon dynamic studies initiated by Bell in support of the XV-3 investigation were followed by several other studies conducted by government and industry over the next decade (see, for example, refs. 3-6). Taken as a whole, these studies helped to establish the technology base needed to later successfully address the issue of proprotor/pylon/wing aeroelastic stability in the design of the XV-15 tiltrotor research aircraft in the mid-1970s and the V-22 Osprey in the mid-1980s.

The mechanism of the proprotor/pylon instability experienced by the XV-3 was identified by Bell during the investigation of that incident and was reported by Hall (ref. 1). The primary destabilizing factor was found to be hub inplane shear forces resulting from rotor precession when operating at high forward speeds in the airplane mode of flight. The hub shears identified as being responsible for the subject instability are actually a subset of a larger set of hub forces and moments that act on a tiltrotor aircraft (ref. 4). Disturbances occurring in flight can excite either the elastic or rigid-body modes of an aircraft in an oscillatory manner. For a tiltrotor aircraft, any motions of this type effectively represent oscillatory translational and rotational motions of the proprotor shaft in space. This leads to proprotor-generated aerodynamic forces and moments that are a function of these oscillatory motions. Figure 1, from reference 4, shows the perturbation rotor-induced aerodynamic forces acting at the hubs of a tiltrotor aircraft executing small pitching and yawing motions when operating in an airplane mode of flight. From the position of these forces on the aircraft, it is clear that the forces shown can influence aircraft longitudinal and lateral-directional stability. However, the shear forces H and Y can, quite independently of any aircraft rigid-body motions, also destabilize the proprotor-pylon-wing system aeroelastically. These are the shear forces identified by Hall (ref. 1) as the drivers for proprotor-pylon instability. They are a direct consequence of airload moments that are generated to precess the rotor in space in response to shaft pitching and yawing motions. In addition to a true whirl instability involving both pitching and yawing motions of the pylon, proprotor/pylon instability can occur in a single plane (either pitch or yaw), depending on the pylon support stiffnesses. Propeller/pylon whirl flutter, on the other hand, is driven by aerodynamic cross-stiffness moments and can occur only if there is pylon flexibility in both pitch and yaw. A discussion of these and other important differences in the aeromechanical behavior of propellers and proprotors is given in reference 4.

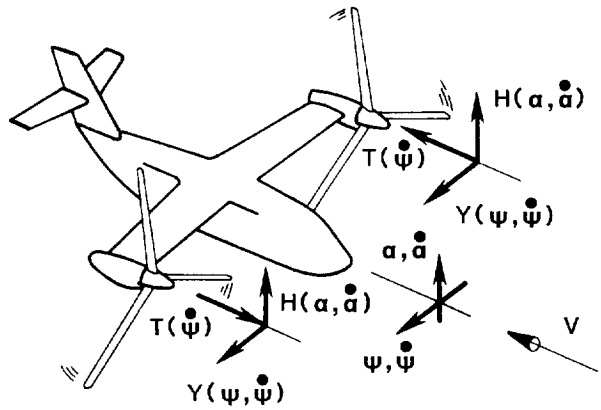

Figure 1. - Perturbation rotor-induced aerodynamic forces acting on a tiltrotor aircraft during pitching and yawing oscillations (rotors interconnected).

Proprotor/pylon aeroelastic stability continues to be a primary consideration in the design of tiltrotor aircraft. Because wing torsional stiffness is the major structural design parameter influencing this phenomenon, the stability requirements of current tiltrotor aircraft (XV-15, V-22, BA-609) have been attained by using thick, torsionally stiff wings having a 23% thickness-to-chord ratio. Such wings provide the torsional stiffness required for stability in those aircraft, albeit at the expense of cruise efficiency and maximum speed. The use of thinner wings would permit higher cruise speeds, increased range, and improved productivity. However, the attendant reduction in wing stiffness would bring with it the problem of proprotor/pylon instability. Thus, aeroelastic instability of the proprotor/pylon/wing system stands as a major barrier to increasing the maximum speed capability of tiltrotor aircraft. Both passive and active methods for extending proprotor/pylon stability boundaries for conventional tiltrotor aircraft have been investigated. References 7-12, which describe studies into the use of wing and blade aeroelastic tailoring techniques for improving stability, are illustrative of passive approaches.

While there have been a number of studies dealing with the use of active controls for improving the aeroelastic behavior of tiltrotor aircraft, most of these have addressed the problem of gust and maneuver load alleviation and there has been only limited attention given to the use of active controls for stability augmentation (refs. 13-16). Reference 13 investigated the application of swashplate feedback for augmentation of aeroelastic stability as part of a broader study of feedback control for improving the aeroelastic and rigid-body flight characteristics of tiltrotor aircraft. The baseline configuration of those studies was a Boeing soft-inplane tiltrotor known as the Model 222. Bode analyses were used to define the appropriate gains and phases

to be applied to the wing responses that were to be fed back to the swashplate cyclic inputs. References 14-15 were analytical studies of feedback control for increasing proprotor/pylon stability on an XV-15 size tiltrotor aircraft. A feedback gain matrix was introduced into the formulation by adding a feedback loop to the equations of motion linearized about a flight condition of interest. Wing tip vertical velocities and accelerations were used for feedback. The gains needed to stabilize the system were determined by simply varying the terms in the gain matrix until an eigenvalue analysis of the closed-loop system indicated a stable system. Reference 16 was an analytical study into the use of linear quadratic regulator (LQR) techniques for determining the wing feedback gains needed to stabilize the whirl modes of a tiltrotor aircraft using an active swashplate. The method was studied using a mathematical model that had been developed earlier for a full-size semi-span configuration of the XV-15. Control design was done in modal space. The discrete state-space equations were transformed to modal form to allow for separation of stable and unstable modes during the design of the controller. A Kalman-Bucy filter was employed as the state estimator to account for disturbances and noise.

The Aeroelasticity Branch (AB) and the Army Research Laboratory's Vehicle Technology Directorate at NASA Langley Research Center, in collaboration with Bell Helicopter Textron Inc (BHTI), is evaluating an adaptive control technique known as Generalized Predictive Control (GPC) (ref. 17) to assess its potential for actively controlling the swashplate of tiltrotor aircraft to enhance aeroelastic stability in both helicopter and airplane modes of flight. The term adaptive as used here refers to a control system in which the parameters describing the model are identified under operational conditions using measured input/output data, and the updated system parameters are then used to compute a new set of control gain matrices and the next set of commands to be sent to the swashplate actuators, with all computations being done on-line. GPC is a time-domain method that uses a linear difference equation to describe the input-output relationship of the system and to design the controller. An ARX-type difference equation is being employed in the present study. The ARX model is used for both system identification and control design. The coefficient matrices of the ARX equation are the quantities determined by the identification algorithm. Closed-loop control is enhanced by performing the system identification in the presence of the external disturbances acting on the system. The coefficients of the ARX model are assembled into a multi-step (finite-horizon) output prediction equation, the desired (target) response is specified, and the resulting expression is used to form an objective function. Minimization of the objective function leads to an expression for the control to be applied to the system.

A 1/5-scale, semispan aeroelastic model of the V-22 designed and built by Bell in 1981 is being used in the experimental evaluation of GPC. That model, on loan to the AB from the Navy, has been refurbished to form a tiltrotor research testbed called the Wing and Rotor Aeroelastic Test System (WRATS) for use in the Langley Transonic Dynamics Tunnel (TDT) (fig. 2).

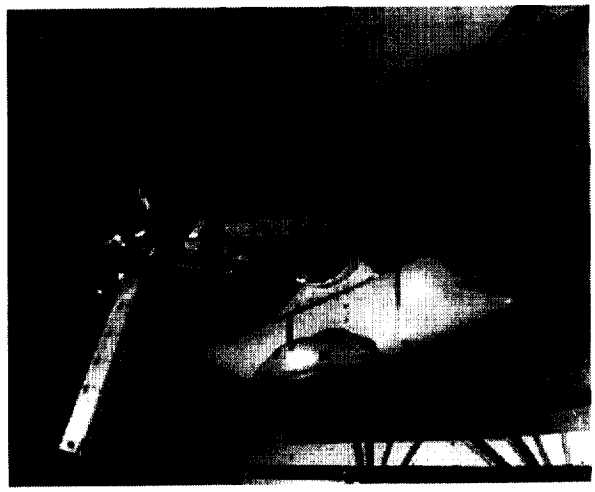

Figure 2. - WRATS tiltrotor testbed installed in TDT.

Three exploratory experimental studies to investigate the use of a multi-input/multi-output (MIMO) GPC-based method for active control have been conducted on the WRATS model to-date (ref. 18). These include a hover test with the baseline stiff-inplane gimbaled rotor (May 1998), a ground resonance test employing a soft-inplane variant of the gimbaled rotor (October 1999), and a wind-tunnel test with the baseline stiffness rotor (April 2000).

The purpose of this paper is to summarize the results of the joint NASA/Army/BHTI investigation that was conducted in the TDT in April 2000 in the initial assessment of the potential of GPC for augmenting stability in tiltrotor aircraft operating in the airplane mode of flight. The WRATS model was modified to incorporate a GPC system for independently controlling the actuators of the fixed-system swashplate. Active control was introduced into the fixed-system swashplate using three high-frequency servo-controlled hydraulic actuators mounted aft of the swashplate inside the pylon fairing. The actuator commands included the steady pilot commands as well as the actuator motions called for by the active control algorithm. Wing bending and torsion strain gages located near the wing root were the sensors used to provide the response measurements needed by the active control algorithm. The GPC-computed commands were summed with the pilot trim commands to produce the desired swashplate actuation about the trim state. The effectiveness of the rotor swashplate in increasing stability (damping) was inves-

tigated over a range of tunnel airspeeds for a single rotor rotational speed. The robustness of the active control system to rapid variations in tunnel airspeed and rotor speed, both singly and in combination, was studied. The effect of GPC on blade loads and pitch link loads was not assessed.

The pertinent equations underlying the method are presented and discussed and the strategy of computer implementation is described, including system identification, calculation of control law matrices, and calculation of the control commands sent to the swashplate actuators. Considerations related to implementation for on-line computations are discussed. Experimental results are then presented illustrating the stability augmentation that was obtained with the GPC-based active control system.

GENERALIZED PREDICTIVE CONTROL

Introductory Remarks

Predictive controllers were initially introduced in the chemical industries for controlling chemical processes and have found applications in a wide variety of industrial processes (e.g., ref. 19). Predictive control refers to a strategy wherein the decision for the current control action is based on minimization of a quadratic objective function that involves a prediction of the system response at some number of time steps into the future. A variety of predictive controllers have been proposed (e.g., ref. 20). Among these, Generalized Predictive Control (GPC), which was introduced in 1987 (ref. 17), has received notable attention by researchers. GPC is a time-domain multi-input-multi-output (MIMO) predictive control method that uses a linear difference equation to describe the input-output relationship of the system. The input-output equation is used to form a multi-step output prediction equation over a finite prediction horizon while subject to controls imposed over a finite control horizon. The control to be imposed at the next time step is determined by minimizing the deviation of the predicted controlled plant outputs from the desired (or target) outputs, subject to a penalty on control effort.

A novel version of the GPC procedure was developed at NASA Langley Research Center in 1997 for efficient computation and unknown disturbance rejection by Dr. Jer-Nan Juang and his co-workers. Their work has resulted in a suite of MATLAB m-files that have been collected into a Predictive Toolbox that can be used by researchers for GPC studies. A summary of the SID and control theory underlying their development is found in references 21-29, among others.

The essential features of the adaptive control process used in the present GPC investigation are depicted in figure 3. The system has r control inputs u, m measured outputs y, and is subject to unknown external

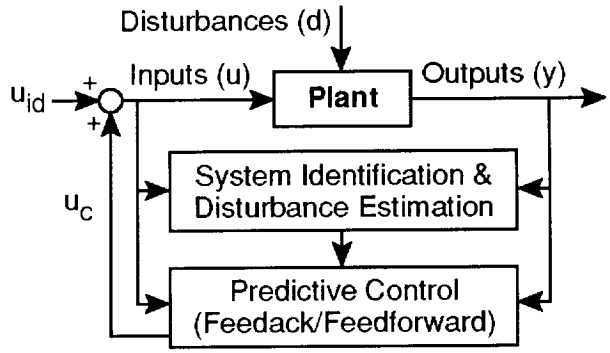

Figure 3. - Block diagram of identification and control procedure.

disturbances d. Measurement noise is also present. There are two fundamental steps involved: (1) identification of the system, and (2) use of the identified model to design a controller. As mentioned earlier, a linear difference equation or model is used to describe the relationship between the input and the output of the system. A linear input-output model gives the current outputs as a linear combination of past input and output measurements. The input-output model used in the present work has the form of what is referred to as an ARX (autoregressive with exogenous input) model. The ARX model is used for both system identification and controller design. System identification is done on-line, but not at every time point, in the presence of any disturbances acting on the system. In this way, an estimate of the disturbance model is reflected in the identified system model and the disturbance does not have to be modeled separately. This approach represents a case of feedback with embedded feedforward. Because the disturbance information is embedded in the feedforward control parameters, there is no need for measurement of the disturbance signal (ref. 28). The parameters of the identified model are used to compute the predictive control law. A random excitation u_{id} (sometimes called dither) is applied initially with u_c equal to zero to identify the open-loop system. Dither is added to the closed-loop control input u_c if it is necessary to re-identify the system while operating in the closed-loop mode.

Form of Model and Control Law Equations

The relationship between the input and output digitized time histories of a MIMO system are described

by an ARX model that has the form

$$y(k) = \alpha_1 y(k\text{-}1) + \alpha_2 y(k\text{-}2) + \cdots + \alpha_p y(k\text{-}p) + \beta_0 u(k) + \beta_1 u(k\text{-}1) + \cdots + \beta_p u(k\text{-}p) \quad (1)$$

This equation states that the current output $y(k)$ at time step k may be estimated by using p sets of the previous output and input measurements, $y(k\text{-}1),\ldots, y(k\text{-}p)$ and $u(k\text{-}1),\ldots,u(k\text{-}p)$; and the current input measurement $u(k)$. The integer p is called the order of the ARX model. The coefficient matrices α_i and β_i appearing in this equation are referred to as observer Markov parameters (OMP) or ARX parameters and are the quantities to be determined by the identification algorithm. Closed-loop robustness is enhanced by performing the system identification in the presence of the external disturbances acting on the system, thereby ensuring that disturbance information will be incorporated into the system model. The goal of SID is to determine the OMP based on input and output data. The OMP may be determined by any SID technique that returns an ARX model of the system.

The ARX model is used to design the controller and leads to a control law that in the case of a regulator problem has the general form given by

$$u_c(k) = \alpha_1^c y(k\text{-}1) + \alpha_2^c y(k\text{-}2) + \cdots + \alpha_p^c y(k\text{-}p) + \beta_1^c u(k\text{-}1) + \beta_2^c y(k\text{-}2) + \cdots + \beta_p^c u(k\text{-}p) \quad (2)$$

Equation 2 indicates that the current control input $u_c(k)$ may be computed using p sets of the previous input and output measurements. The coefficient matrices α^c and β^c appearing in this equation are the control gain matrices.

System Identification

System identification in the presence of the operational disturbances acting on the system is the first of the two major computational steps. The external disturbances acting on the system are assumed to be unknown (unmeasurable). The number of control inputs is r and the number of measured outputs is m. The system is excited with band-limited white noise for SID. These random excitations are input to all r control inputs simultaneously and the m responses are measured. The digitized input and output time histories (u and y) at l time points are then used to form the data matrices y and V in the equation

$$y = \overline{Y}\, V \quad (3)$$

where

$$\underset{m\times l}{y} = \begin{bmatrix} y(0) & y(1) & y(2) \cdots y(p) \cdots y(l-1) \end{bmatrix} \quad (4)$$

and

$$\underset{[r+(r+m)p]\times l}{V} = \begin{bmatrix} u(0) & u(1) & u(2) & \cdots & u(p) & \cdots & u(l-1) \\ & v(0) & v(1) & \cdots & v(p-1) & \cdots & v(l-2) \\ & & v(0) & \cdots & v(p-2) & \cdots & v(l-3) \\ & & & \ddots & \vdots & \cdots & \vdots \\ & & & & v(0) & \cdots & v(l-p-1) \end{bmatrix} \quad (5)$$

Equations 4 and 5 follow from writing the discrete-time state-space equations for a linear time-invariant system at a sequence of time steps $k = 0, 1,\ldots, l\text{-}1$ and grouping them into matrix form. The vector $v(k)$ appearing in the data matrix V is formed from the vectors $u(k)$ and $y(k)$ according to

$$\underset{(r+m)\times 1}{v(k)} = \begin{Bmatrix} u(k) \\ y(k) \end{Bmatrix} \quad (6)$$

The order of the ARX model (p) and the number of time steps (l) must be specified by the user. Some guidelines for their selection are given later. The sizes of the vectors and arrays are noted.

In forming the matrices given in equations 4 and 5, it has been assumed that the state matrix A is asymptotically stable so that for some sufficiently large p, $A^k \approx 0$ for all time steps $k \geq p$, and that an observer has been added to the system. It is through these expedients that the matrix V is reduced to a size amenable for practical numerical computation of its pseudo-inverse. The SID process yields OMP rather than system Markov parameters (SMP) because of the inclusion of an observer. A complete discussion of these aspects of the development may be found in reference 21.

$\overline{Y}$ is the matrix of observer Markov parameters that are to be identified and has the form

$$\underset{m\times[r+(r+m)p]}{\overline{Y}} = \begin{bmatrix} \underset{m\times r}{\beta_0} & \underset{m\times r}{\beta_1} & \underset{m\times m}{\alpha_1} & \underset{m\times r}{\beta_2} & \underset{m\times m}{\alpha_2} & \underset{m\times r}{\beta_3} & \underset{m\times m}{\alpha_3} & \cdots & \underset{m\times r}{\beta_p} & \underset{m\times m}{\alpha_p} \end{bmatrix} \quad (7)$$

The solution for $\overline{Y}$ is obtained by solving equation 3 for $\overline{Y}$ according to

$$\overline{Y} = \mathrm{y}\, V^{\dagger} = \mathrm{y}\, V^{T}\left[V\ V^{T}\right]^{-1} \tag{8}$$

where † denotes the pseudo-inverse. If the product $V\ V^T$ is a well-conditioned matrix of reasonable size, the ordinary inverse can be taken as shown. Otherwise, a pseudo-inverse must be used. It should be noted that because the size of $V\ V^T$ is much smaller than V, a pseudo-inverse might be appropriate even if the product is well conditioned.

Multi-Step Output Prediction Equation

The one-step ahead output prediction equation given in equation 1 is the starting point for deriving the multi-step output prediction equation that is needed for designing a GPC controller. Using equation 1, the output at time step $k+j$ may be written in the form

$$\begin{aligned} y(k+j) = {} & \alpha_1^{(j)} y(k\text{-}1) + \alpha_2^{(j)} y(k\text{-}2) + \cdots + \alpha_p^{(j)} y(k\text{-}p) \\ & + \beta_0 u(k+j) + \beta_o^{(1)} u(k+j-1) + \cdots + \beta_o^{(j)} u(k) \\ & + \beta_1^{(j)} u(k\text{-}1) + \beta_2^{(j)} u(k-2) + \cdots + \beta_p^{(j)} u(k\text{-}p) \end{aligned} \tag{9}$$

where the coefficient matrices are given by recursive expressions involving the matrices α_i and β_i appearing in the ARX equation (ref. 25). The system identification process described earlier determines the matrices α_i and β_i. Equation 9 shows that the output $y(k+j)$ at time step $k+j$ may be estimated by using p sets of the previous output and input measurements, $y(k\text{-}1),\ldots,\ y(k\text{-}p)$ and $u(k\text{-}1),\ldots,u(k\text{-}p)$, and the (unknown) current and future inputs, $u(k),\ u(k+1),\ldots,u(k+j)$. The GPC algorithm is based on system output predictions over a finite horizon h_p known as the prediction horizon. To predict future plant outputs, some assumption needs to be made about future control inputs. In determining the future control inputs for GPC, it is assumed that control is applied over a finite horizon h_c known as the control horizon. Beyond the control horizon the control input is assumed to be zero. In GPC, the control horizon is always equal to or less than the prediction horizon. Letting j in equation 9 range over the set of values $j = 1, 2, \ldots, h_p\text{-}1$, the resulting equations can be assembled into a multi-step output prediction equation having the form

$$\underset{h_p m\times 1}{y_{h_p}(k)} = \underset{h_p m\times h_c r}{\mathcal{T}}\ \underset{h_c r\times 1}{u_{h_c}(k)} + \underset{h_p m\times pr}{\mathcal{B}}\ \underset{pr\times 1}{u_p(k-p)} + \underset{h_p m\times pm}{\mathcal{A}}\ \underset{pm\times 1}{y_p(k-p)} \tag{10}$$

The coefficient matrices $\mathcal{T}$, $\mathcal{B}$, and $\mathcal{A}$ are formed from combinations of the observer Markov parameters α_i and β_i. The quantity $y_{hp}(k)$ is the vector containing the future outputs, whereas $u_{hc}(k)$ is the vector containing the future control inputs yet to be determined. The quantities $u_p(k\text{-}p)$ and $y_p(k\text{-}p)$ are vectors containing the previous p sets of control inputs and outputs, respectively. The expanded form of this multi-step output prediction equation is shown in equation 11.

$$\boxed{\beta_0^{(q)} = \beta_1^{(q-1)} + \alpha_1^{(q-1)}\beta_0}$$

$$\begin{Bmatrix} y(k) \\ y(k+1) \\ \vdots \\ y(k+q-1) \\ y(k+q) \\ \vdots \\ y(k+h_p-1) \end{Bmatrix} = \begin{bmatrix} \beta_o & & & \\ \beta_o^{(1)} & \beta_o & & \\ \vdots & \vdots & \ddots & \\ \beta_o^{(q-1)} & \beta_o^{(q-2)} & \cdots & \beta_o \\ \beta_o^{(q)} & \beta_o^{(q-1)} & \cdots & \beta_o^{(1)} \\ \vdots & \vdots & \ddots & \vdots \\ \beta_o^{(h_p-1)} & \beta_o^{(h_p-2)} & \cdots & \beta_o^{(h_p-h_c)} \end{bmatrix} \begin{Bmatrix} u(k) \\ u(k+1) \\ \vdots \\ u(k+h_c-1) \end{Bmatrix} \qquad h_C \le h_p$$

$$+ \begin{bmatrix} \alpha_1 & \alpha_2 & \cdots & \alpha_{p-1} & \alpha_p \\ \alpha_1^{(1)} & \alpha_2^{(1)} & \cdots & \alpha_{p-1}^{(1)} & \alpha_p^{(1)} \\ \vdots & \vdots & \ddots & \vdots & \vdots \\ \alpha_1^{(q-1)} & \alpha_2^{(q-1)} & \cdots & \alpha_{p-1}^{(q-1)} & \alpha_p^{(q-1)} \\ \alpha_1^{(q)} & \alpha_2^{(q)} & \cdots & \alpha_{p-1}^{(q)} & \alpha_p^{(q)} \\ \vdots & \vdots & \ddots & \vdots & \vdots \\ \alpha_1^{(h_p-1)} & \alpha_2^{(h_p-1)} & \cdots & \alpha_{p-1}^{(h_p-1)} & \alpha_p^{(h_p-1)} \end{bmatrix} \begin{Bmatrix} y(k-1) \\ y(k-2) \\ \vdots \\ y(k-p+1) \\ y(k-p) \end{Bmatrix} + \begin{bmatrix} \beta_1 & \beta_2 & \cdots & \beta_{p-1} & \beta_p \\ \beta_1^{(1)} & \beta_2^{(1)} & \cdots & \beta_{p-1}^{(1)} & \beta_p^{(1)} \\ \vdots & \vdots & \ddots & \vdots & \vdots \\ \beta_1^{(q-1)} & \beta_2^{(q-1)} & \cdots & \beta_{p-1}^{(q-1)} & \beta_p^{(q-1)} \\ \beta_1^{(q)} & \beta_2^{(q)} & \cdots & \beta_{p-1}^{(q)} & \beta_p^{(q)} \\ \vdots & \vdots & \ddots & \vdots & \vdots \\ \beta_1^{(h_p-1)} & \beta_2^{(h_p-1)} & \cdots & \beta_{p-1}^{(h_p-1)} & \beta_p^{(h_p-1)} \end{bmatrix} \begin{Bmatrix} u(k-1) \\ u(k-2) \\ \vdots \\ u(k-p+1) \\ u(k-p) \end{Bmatrix} \tag{11}$$

$$\boxed{\alpha_{p-1}^{(q)} = \alpha_p^{(q-1)} + \alpha_1^{(q-1)}\alpha_{p-1}} \qquad \boxed{\beta_{p-1}^{(q)} = \beta_p^{(q-1)} + \alpha_1^{(q-1)}\beta_{p-1}}$$

The OMP α_i and β_i determined in SID form the first block rows of the coefficient matrices $\mathcal{T}$, $\mathcal{A}$, and $\mathcal{B}$ in equation 11. The terms in the remaining rows are computed using the recursive relations indicated in the boxes (ref. 25). All terms in equation 11 are known, except for the h_c sets of future commands and the h_p sets of predicted responses. The goal of the GPC control algorithm is to determine the set of future commands $u(k)$, $u(k+1)$, ..., $u(k+h_c-1)$ that are required to achieve a desired predicted response $y(k)$, $y(k+1)$, ..., $y(k+h_p-1)$.

It should be remarked that the system Markov parameters (SMP), which are commonly used as the basis for identifying discrete-time models for linear dynamical systems, form the first block column in the matrix $\mathcal{T}$; the remaining block columns are formed from subsets of the SMP. The Markov parameters are the pulse response of a system and are unique for a given system. The discrete-time state-space matrices A, B, C, and D are embedded in the SMP.

Derivation of Control Law

The predictive control law is obtained by minimizing the deviation of the predicted controlled response (as computed from the multi-step output prediction equation) from a specified target response over a prediction horizon h_p. To this end, one first defines an error function that is the difference between the desired (target) response $y_T(k)$ and the predicted response $y_{h_p}(k)$:

$$\begin{aligned}\varepsilon &= y_T(k) - y_{h_p}(k) \\ &= y_T(k) - \mathcal{T} u_{h_c}(k) - \mathcal{B} u_p(k-p) - \mathcal{A} y_p(k-p)\end{aligned} \tag{12}$$

An objective function J quadratic in the error and the unknown future controls is then formed:

$$J = \varepsilon^T R \varepsilon + u_{h_c}^T Q\, u_{h_c} \tag{13}$$

Two weighting matrices are included in the objective function: Q (symmetric and positive definite) is used to weight the control effort and stabilize the closed-loop system; R (symmetric and positive semi-definite) is used to weight the relative importance of the differences between the target and predicted responses. Typically, Q and R are assumed to be diagonal and for Q to have the same value w_c along its diagonal and R to have the same value w_r along its diagonal. Minimizing J with respect to $u_{h_c}(k)$ and then solving for $u_{h_c}(k)$ gives

$$\begin{aligned}u_{h_c}(k) &= -(\mathcal{T}^T R \mathcal{T} + Q)^{\dagger} \mathcal{T}^T R \left(-y_T(k) + \mathcal{B} u_p(k-p) + \mathcal{A} y_p(k-p)\right) \\ &= \underset{h_c r \times 1}{\gamma} \left(-y_T(k) + \mathcal{B} u_p(k-p) + \mathcal{A} y_p(k-p)\right)\end{aligned} \tag{14}$$

as the control sequence to be applied to the system over the next h_c time steps. However, only the first r values (corresponding to the first future time step)

$$\underset{r \times 1}{u_c(k)} = -\gamma^c y_T(k) + \beta^c u_p(k-p) + \alpha^c y_p(k-p) \tag{15}$$

are applied to the r control inputs, the remainder are discarded, and a new control sequence is calculated at the next time step.

The target response is zero for a regulator problem and non-zero for a tracking problem. The matrix Q must be tuned to ensure a stable closed-loop system. Typically, h_c is chosen equal to h_p. However, h_c may be chosen less than h_p resulting in a more stable, but sluggish, regulator.

An expression for estimating the order of the ARX model that is to be used for SID is given by

$$p \geq ceil\left(\frac{\dfrac{number\ of}{system\ states} + \dfrac{number\ of}{disturbance\ states}}{m}\right) \tag{16}$$

where *ceil* denotes rounding up the value of the quantity in parentheses to the next higher integer. The number of system states is typically chosen to be twice the number of significant structural modes; the number of disturbance states is set to twice the number of frequencies in the disturbance; m is the number of output measurements. If measurement noise is of concern, the order of p so computed should be increased to allow for computational poles and zeros to improve system identification in the presence of noise. In practice, simply choosing p to be 5-6 times the number of significant modes in the system is often adequate. The prediction and control horizons are set according to the relations

$$h_p \geq p \qquad h_c \leq h_p \tag{17}$$

Although h_p can be set equal to p, h_p is typically set greater than p to weight the control effort so as not to saturate the control actuators. If the control horizon is greater than the system order a minimum energy (minimum norm) solution is obtained wherein the commanded output is shared so that the control actuators don't fight each other. If h_p is set equal to p one obtains

a so-called deadbeat controller (ref. 25). By extending the prediction and control horizons (and hence p, the order of the ARX model) to very large values, the GPC solution approaches that of the linear quadratic regulator (LQR). Thus, GPC approximates an optimal controller for large p (ref. 17).

Weighting matrices Q and R are used to weight the control effort and to weight the relative importance of the differences between the target and predicted responses, respectively. As mentioned earlier, Q and R are usually assumed to be diagonal and for Q to have the same value w_c along its diagonal and R to have the same value w_r along its diagonal. The control weight must be tuned to produce an acceptable solution without going unstable. Reducing w_c increases control authority and performance but eventually drives the system unstable.

Key Features of Present Method

An ARX model is employed to represent the system and is used for both system identification and controller design. The SID process used makes recourse to an observer to enable numerical computation of the pseudo-inverse needed for calculation of the OMP that comprise the coefficients of the ARX equation. The controller is thus inherently observer-based but no explicit consideration of the observer needs to be taken into account in the implementation. In practice, the disturbances acting on the system are unknown or unmeasurable. However, as discussed in reference 28, by performing the SID in the presence of the external disturbances acting on a system, a disturbance model is implicitly incorporated into the identified observer Markov parameters. However, the identified model must be larger than the true system model to accommodate the unknown disturbances. Thus, the effects of the unknown disturbances acting on the system are embedded in the matrices $\mathcal{A}$ and $\mathcal{B}$, and hence the control law matrices α^c and β^c. If only the disturbances acting on the system change, there is no need to recalculate $\mathcal{T}$ (and hence γ^c) because $\mathcal{T}$ is formed solely from the SMP, which are unique for a given system (ref. 28). The solution for $\overline{Y}$ indicated in equation 8 involves forming the matrix products yV^T and VV^T. Here, these products are obtained using the computationally efficient procedure described in reference 23.

Computational Considerations

Several considerations dealing with computations should be kept in mind when developing algorithms for GPC applications.

SID should be done with the external disturbances acting on the system so that information about the disturbances is embedded in the OMP. However, depending on the nature of the external disturbances, it may be possible to perform a SID on a system without the external disturbances and still determine a control law that results in satisfactory closed-loop performance.

The computation of pseudo-inverses should be performed using Singular Value Decomposition (SVD) because of the latter's ability to deal with matrices that are numerically ill conditioned. The use of pseudo-inverses (via SVD) is recommended even in cases where the ordinary inverse may seem appropriate (such as in the operation $(VV^T)^{-1}$ indicated in equation 8).

A number of decisions also need to be made. For example, should the system be re-identified and the control law matrices recalculated in every sampling period, every specified number of time steps (block updating), or only if some event requiring a re-ID occurs? Should all the calculations be done in real time, or can some be done in near real time? Should updating of the OMP be done in batch mode or recursively?

Microprocessor speeds are such that it is now often possible to complete the full cycle of GPC computations and apply the commands to the actuators within one sampling period. However, the need for efficient computational algorithms and attendant coding is not expected to diminish.

Implementation Considerations

Several considerations must be taken into account when actually implementing GPC algorithms in hardware for active controls work.

The measured response time histories must be passed through a low-pass filter with a cut-off frequency set equal to the Nyquist frequency f_N. The latter is chosen so that the maximum frequency of interest is about 75% of f_N. The sampling frequency f_S should be at least twice f_N to prevent aliasing. However, if f_S is made too large the low frequency modes will be poorly identified due to a loss of frequency resolution. A sampling rate between 2 to 3 times f_N is generally sufficient. Once the sampling frequency has been selected, the minimum number of data points that should be used for SID follows from the requirement of having 5-10 cycles of the lowest frequency mode in the measured response time histories. Normalization of the input and output data that is used for SID on the maximum actual or expected values of the data is often helpful numerically. The procedure will depend on whether the computations are being done in batch mode or recursively.

The computing tasks can be distributed among computers or different CPUs on a single computer. The choice will influence the extent of user involvement. The values of the input and output data that are being used during closed-loop operations must be carefully monitored to ensure that they fall within acceptable bounds. This is easily done using IF/THEN-type checks in the code.

EXPERIMENTAL SETUP

Wind Tunnel

The experiment was conducted in the Langley Transonic Dynamics Tunnel, which is a continuous flow, single return, variable pressure tunnel having a test section 16-feet square with cropped corners. The control room and test section walls are provided with large windows for close viewing of the model. The tunnel is capable of operation at stagnation pressures from near vacuum to slightly above atmospheric and at Mach numbers from near zero up to about 1.2. Either air or a heavy gas (R-134a) can be used as the test medium. Both the density and test-section Mach number are continuously controllable. The present investigation was conducted in air near atmospheric conditions and at free-stream Mach numbers less that 0.30.

Model

The model used in the investigation is a modified version of a Froude-scaled semispan aeroelastic model of the V-22 tiltrotor that was used by Bell/Boeing to support the preliminary and full-scale design phases of the aircraft (Ref. 30). Upon completion of that series of tests, the Navy transferred the model to the Aeroelasticity Branch (AB) at NASA Langley under a loan agreement to be used as the experimental testbed of a tiltrotor aeroelastic research program that was initiated by AB in 1994. The tiltrotor testbed has been designated the Wing and Rotor Aeroelastic Testing System (WRATS).

General Characteristics

The WRATS tiltrotor testbed as installed in the Langley Transonic Dynamics Tunnel for this study is shown in figure 2. The model has a length scale factor of 1/5 and was designed to maintain full-scale values of the Froude, Lock, and Strouhal numbers when operated in air (Ref. 30). The wing and rotor are dynamically and aeroelastically scaled; the pylon is only dynamically scaled. The fuselage is rigid and only maintains the scaled external aerodynamic shape. The model is attached to a support structure that is effectively rigid, its lowest frequency being well above any important elastic mode frequency of the model. Simulation of the distributed wing beamwise, chordwise, and torsional stiffness is provided by means of a hollow, rectangular cross section, composite spar having chordwise flanges. The 4.6-foot spar, which lies along the calculated elastic axis of the wing, has segmented, nonstructural, aluminum aerodynamic fairings that provide the spanwise distribution of airfoil contour. To provide surface continuity over the lifting surface of the wing, the space between the segments is filled with strips of foam rubber. The wing-tip-mounted pylon contains the transmission and gearbox components for the rotor drive system, the lower part of the mast, and the swashplate control system. Because these internal components can be treated as rigid, the pylon is scaled dynamically so as to preserve its overall mass and inertia properties. The pylon is attached to the wing tip by means of a "racetrack" spring assembly that simulates the combined stiffness of the full-scale conversion actuator and downstop lock mechanism.

The 3-bladed, 7.6-foot diameter stiff-inplane rotor has a gimbaled hub that is connected to the mast by a constant speed joint (2 coincident universal joints). The rotor yoke has 2.5 degrees of built-in precone and is flexible to allow the blade coning angle to adjust under centrifugal loading. The blades have a nonlinear distribution of built-in twist with an overall root-to-tip twist of 47.5 degrees (leading edge down).

A large plywood panel through the vertical plane of symmetry of the model and attached to a support structure consisting of a spider-like arrangement of steel tubes was employed to seal the open back side of the semi-fuselage and to serve as a reflection plane. The structure also provided the offset needed to position the rotor axis near the centerline of the wind tunnel.

The fundamental natural frequencies of the model (as measured on the test stand) with the pylon locked to the downstop in an airplane mode configuration are summarized in Table I. Typical wind-on natural

Table I - System Natural Frequencies*

Mode	Frequency, Hz
Wing Beam Bending	5.83
Wing Chord Bending	8.67
Wing Torsion	12.0
Pylon Yaw (2nd wing chord)	19.4
Blade 1st Elastic Flap	7.20
Blade 1st Elastic Lag	12.5
Blade Rigid Body Torsion	95.6
Blade 1st Elastic Torsion	110.

* Rotor on, flapping locked out, zero rpm.

frequencies of the rotor system (e.g., at V=100 knots and Ω = 742 rpm) are: gimbal flapping at 0.85P, first cyclic lag at 1.2P, and collective flapping (coning mode) at about 1.7 P. The present test was run with the drive system disconnected so the collective lag mode had zero frequency.

Active Swashplate Hardware

Three high-frequency electro-hydraulic actuators having a bandwidth of 50 Hertz were used in the control system to drive the swashplate (fig. 4). The actuators are positioned azimuthally at the 12, 4, and 8 o'clock positions around and slightly aft of the nonrotating swashplate. These actuators were used to input the steady pilot commands as well as the swashplate inputs called for by the GPC active control algorithm. Three 3000-psi servo-valves were used to meter hydraulic fluid to the actuators. These servo-valves were located inside the pylon near their corresponding actuators (see fig. 4).

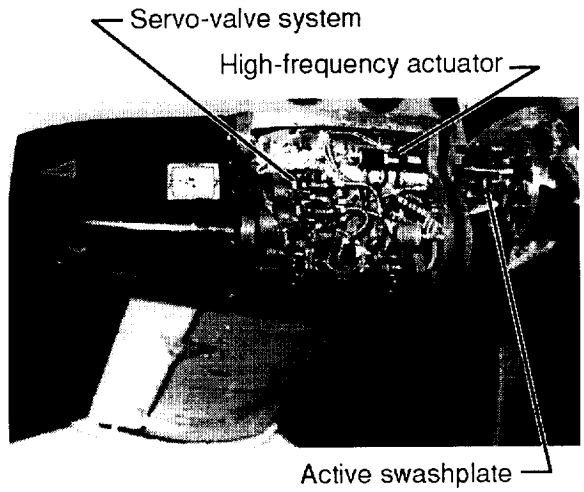

Figure 4. - Major hardware components of the GPC active control system.

Feedback Signals and Instrumentation

Feedback signals for the active control system were developed from the measured responses of the pylon/wing system. The suite of candidate responses included wing strain gages (beam, chord, and torsion) and six pylon accelerations (normal, lateral, and axial). The beam and chord strain gages are located 17.0 inches out from the root and the torsion strain gages are located 23.0 inches out from the root. The wing bending and torsion gages were the sensors used for feedback. A number of other measurements were monitored and recorded either to trim the rotor or for flight safety, including gimbal flapping angles and downstop spring load. Pitch-link and blade loads were not measured.

Control System Architecture

A schematic diagram of the control system for active stability augmentation is shown in figure 5. The flapping response of the rotor is displayed

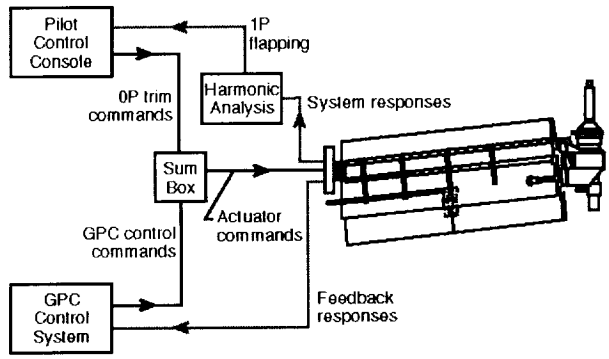

Figure 5. - Schematic of active stability control system.

to the pilot as 1P lateral and longitudinal flapping of the rotor tip-path-plane. The pilot trims the windmilling rotor by setting both the collective pitch (to maintain the desired rotor speed) and the cyclic pitch (to maintain zero flapping with respect to the shaft). A mixer in the pilot control console calculates the commands to be sent to the individual actuators to trim the rotor based on the pilot stick commands. The GPC control system calculates the actuator commands needed for stability augmentation. The steady 0P (DC) swashplate actuator commands required for trim are summed with the oscillatory actuator commands calculated by the GPC system (after those commands are converted from digital to analog signals).

Data Acquisition and Processing

The data acquisition system (DAS) that is part of the WRATS testbed is a 64-channel, PC-based system consisting of a National Instruments data acquisition board housed in a 750 MHz Pentium processor computer with a per-channel sampling rate of 1000 Hz. The WRATS DAS is controlled using a LabVIEW front panel that has been customized to support WRATS model testing. LabVIEW applications have been developed for on-line FFT analyses, harmonic analyses, exciting the model via stick-stir inputs to the swashplate, damping estimations using moving block and logarithmic decrement analyses, and plotting. The digitized data records are written in a binary file format to the

host PC's hard disk for access during the test and to CDs for permanent storage. A MATLAB-based program is used for post-test data reduction and plotting.

The GPC computer consisted of a 500 MHZ dual processor PC that included a dSPACE DSP1103 add-in card for performing real-time data acquisition and computations. A sampling rate of 100 Hz was used for the GPC data channels. The GPC computational tasks were distributed among these three computing elements in the manner indicated in figure 6. The entire process was managed using ControlDesk, dSPACE's graphical user interface (GUI), which was installed on CPU #2. The portion of the GPC algorithm that computes the control gain matrices α^c and β^c is written in MATLAB and runs on CPU #1. The calculation of the control inputs u_c that are sent to the swashplate actuators is made by executable code that is installed on the DSP card. This code is generated by using Real-Time Workshop to convert a Simulink block diagram of the control law calculation to C code. The C code then goes to the dSPACE compiler, which generates the executable code that is placed on the DSP. The user specifies appropriate values for the parameters l, p, h_p, h_c, w_c, and w_r needed by the GPC algorithm and initializes the control gain matrices α^c and β^c to zero using the ControlDesk front panel GUI that runs on CPU #2. The DSP card continuously collects the r-input and m-output data sets used by the GPC algorithm. On user command, the DSP sends the set of input/output data needed for system identification to CPU #1 where the SID computations are performed and the control gain matrices α^c and β^c are computed. The control gain matrices are automatically sent to the DSP, which uses the p latest data sets to (continuously) compute the control commands to be sent to the swashplate actuators. Re-identification of the system, if needed, is done closed-loop and on user command.

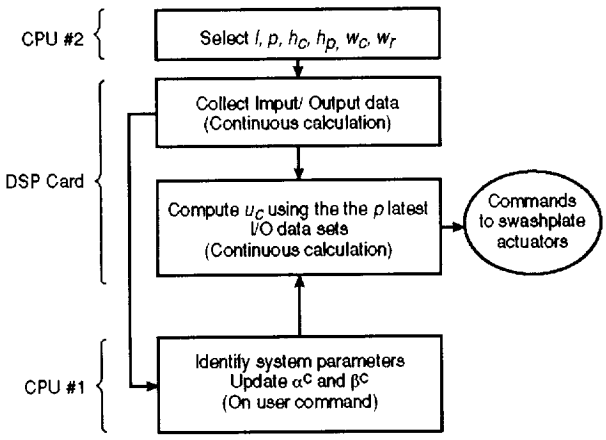

Figure 6. - Distribution of computing tasks in GPC computer for active control studies.

Test Conditions and System Configurations

The GPC investigation constituted only a portion of a much broader aeroelastic investigation that was conducted with the WRATS model during the April 2000 test in the TDT. One of the other objectives of that test was to establish new baseline stability boundaries for the model that included the hydraulic components that had been installed earlier for active controls testing. This baseline stability investigation was conducted with the pylon in both the on- and off-downstop configurations, over a range of rotor rpm, in both air and heavy gas.

All GPC testing was conducted with the pylon oriented in the airplane mode of flight and locked to the wing downstop. The rotor was unpowered (windmilling). The stability of the model with the GPC-based algorithm was measured over a range of tunnel airspeeds up to a maximum of 120 kt, for a single rotor rotational speed (888 rpm), and two values of kinematic pitch-flap coupling (δ_3) angles ($-15°$ and $-45°$). Because this was the first wind-tunnel test of the GPC algorithm, a conservative approach was adopted wherein all closed-loop testing was conducted at conditions that were slightly within (more stable than) the corresponding open-loop stability boundaries.

Test Procedure

The primary pylon/wing structural frequencies of interest lie between 4 and 25 Hz, with the critical wing beam mode frequency varying from 5.8 Hz down to as low as 4.5 Hz with increasing airspeed. Based on the implementation guidelines discussed earlier, the Nyquist frequency f_N was taken as 30 Hz, the sampling frequency f_S was set to 100 Hz, and the number of time steps l of input/output data used for SID was taken as 300.

For this test, the control horizon h_c was set equal to the prediction horizon h_p, h_p was set equal to p, the order of the ARX model, and the response weight w_r was set to unity. The assumed order of the ARX model (p) and the control weight (w_c) were varied to tune the controller to the nuances of the WRATS model in the on-downstop configuration with $\delta_3 = -15°$ while operating at an airspeed of 80 kt, which is well below the open-loop flutter speed of that configuration. The tuning process was conducted at both 770 and 888 rpm and led to the selection of the following best values for these quantities: $p = 30$ and $w_c = 1.0$. Active control was introduced into the fixed-system swashplate using three hydraulic servo-actuators mounted aft of the swashplate inside the pylon fairing. Wing bending (vertical and chordwise) and torsion strain gages located near the

wing root were the sensors used to provide the response measurements needed by the active control algorithm. Thus, there were three control inputs (r = 3) and three feedback outputs (m = 3).

In addition to its use to actively control the rotor for GPC stability augmentation, the active swashplate was also used to impose "stick stirs" to excite the wing modes of interest for damping determination. These stick-stir commands were superimposed on the GPC and pilot control commands sent to the swashplate actuators. Control of the stick stir is integrated into the GUI that is part of the WRATS DAS software. The procedure employed for the GPC testing is as follows: (1) With GPC off, the tunnel airspeed is brought up to a selected value; (2) GPC is turned on (the associated reduction in model response is visibly quite dramatic); (3) Data acquisition is initiated; (4) A stick-stir excitation is imposed at the frequency of the wing mode of interest; (5) The resulting wing beam (or other) response is observed visually by the test engineer and the stir terminated when sufficient amplitude has been attained; (6) The response is allowed to decay freely to its steady-state value ; and (7) Data acquisition is turned off. The total data acquisition time is typically 5-8 seconds long. The free-decay portion of the recorded time history is then analyzed by moving block and log decrement methods to obtain an estimate for the modal damping and the damped natural frequency. This process is repeated until five acceptable estimates of the damping are obtained. GPC is then turned off and the entire procedure beginning with step (1) is repeated for all of the airspeeds of interest.

The performance and robustness of the GPC algorithm were assessed in transient conditions for δ_3 = −15° by rapidly changing tunnel airspeed and rotor rotational speed, both singly and in combination. The rotor speed was varied between 770 and 888 rpm and the tunnel airspeed between 60 and 145 kt.

RESULTS AND DISCUSSION

The GPC-based active control system was found highly effective in increasing the stability (damping) of the critical wing mode for all of the configurations of the model tested. In particular, GPC was able to consistently yield a closed-loop system in which the critical wing mode had a minimum of about four-percent modal damping over the range of test conditions investigated, without visible degradation of the damping in the other modes. The algorithm was robust with respect to its performance in the tracking of rapid changes in both the rotor speed and the tunnel airspeed. System identification done at a low-speed flight condition was generally sufficient for a wide range of rotor speeds and tunnel velocities.

An indication of the effectiveness of the GPC-based active control system in increasing the stability (damping) of the critical wing beam mode of the model is given in figures 7 and 8. The figures show a comparison of the measured open-loop and closed-loop wing beam mode damping versus airspeed for δ_3 values of −45° and −15°, respectively. The mean and standard

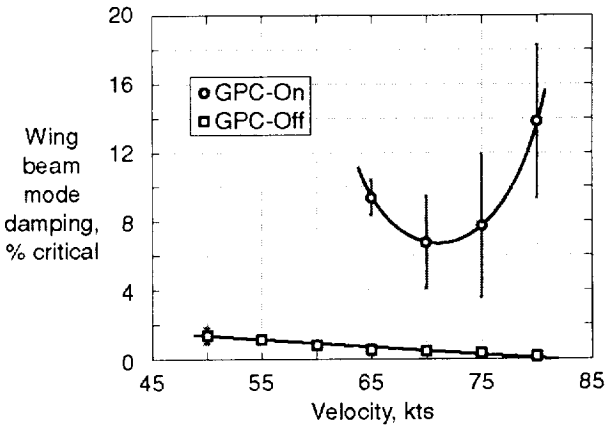

Figure 7. - Comparison of wing beam mode damping versus airspeed with GPC on and off for δ_3 = −45°.

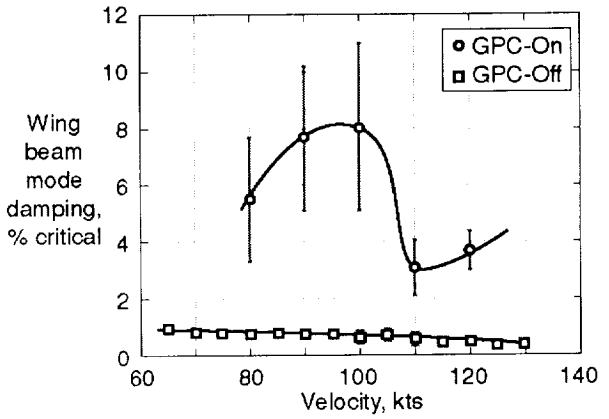

Figure 8. - Comparison of wing beam mode damping versus airspeed with GPC on and off for δ_3 = −15°.

deviation of the five values of damping that were measured at each airspeed were determined. The mean values of damping are indicated by the symbols, and the vertical lines indicate the standard deviations about

these mean values. The plotted curves are the result of a spline fit applied to the mean values. As can be seen, with GPC turned on the wing beam mode damping is considerably higher than with GPC off over the entire range of tunnel airspeeds tested. It should be remarked that with GPC on, it was often difficult to estimate the damping from the free-decay responses after termination of the stick-stir because the large damping levels resulted in very few cycles of motion (sometimes as few as one or two) being available for the damping calculations. This is the reason for the large standard deviation in the measured values of the closed-loop damping. In contrast, because the open-loop damping of the wing beam mode is small, the standard deviation of the measured damping is correspondingly very small. It should also be remarked that the effectiveness of GPC was such that it tried to quell the imposed stick-stir excitation, thus requiring considerable amplitude of excitation. The reason for the drop-off and then rise in closed-loop damping at 100 knots in figure 8 is not known.

The measured time histories of the wing beam bending moments during and after a typical stick-stir excitation with GPC on and off are shown in figures 9 and 10. Figure 9 corresponds to the 75-knot airspeed of figure 7 and figure 10 corresponds to the 120-knot airspeed of figure 8. The closed-loop time histories clearly illustrate the effectiveness of the GPC-based active control system to rapidly reduce the response.

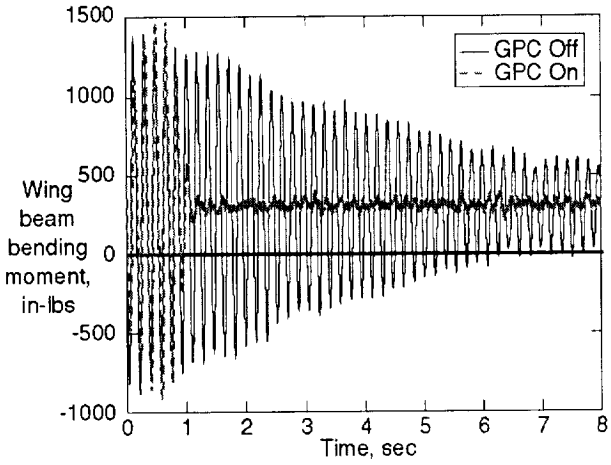

Figure 9. - Effect of GPC on damped response of wing beam bending mode at 75 kt for $\delta_3 = -45°$.

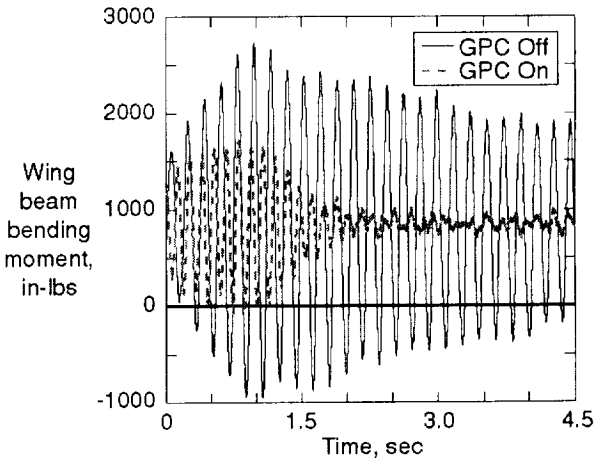

Figure 10. - Effect of GPC on damped response of wing beam bending mode at 120 kt for $\delta_3 = -15°$.

Another example of the effectiveness of GPC is given in figure 11, which shows a time history of the wing beam bending moment while repeatedly cycling GPC on and off for the 120-knot airspeed case of figure 8. The response is seen to adapt quickly to the changing conditions, suggesting a certain level of robustness.

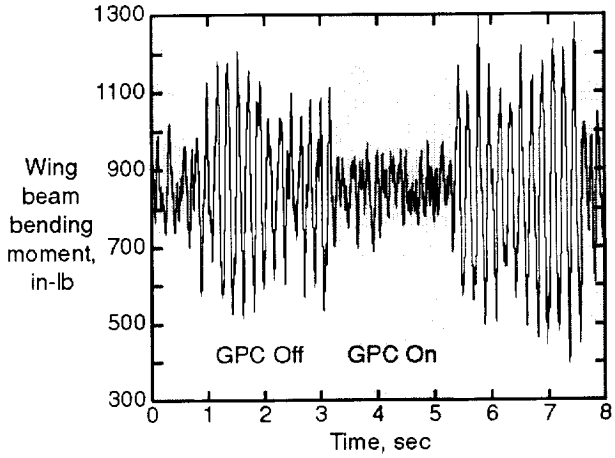

Figure 11. - Time history of wing beam bending moment while cycling GPC on and off at 120 kt for $\delta_3 = -15°$.

An indication of the swashplate pitch angles that are associated with the GPC commanded actuator inputs is given in figure 12. The figure shows the time history of the longitudinal and lateral cyclic pitch angles for the 120-knot airspeed condition of figure 8 from a time near

the end of a stick-stir excitation to a time well into the steady-state condition. The steady-state oscillatory cyclic pitch angles are seen to be modest.

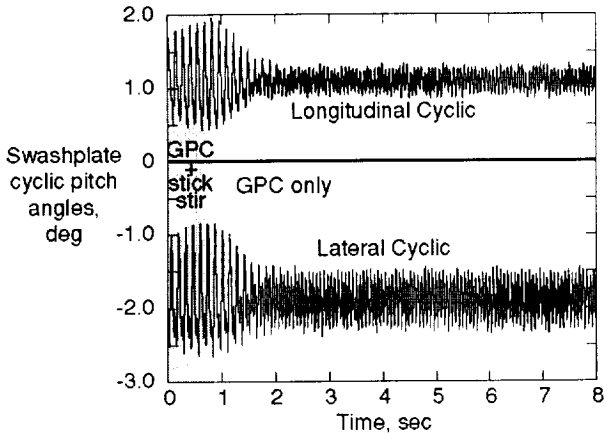

Figure 12. - Measured time histories of closed-loop swashplate cyclic pitch angles at 120 kt for $\delta_3 = -15°$.

CONCLUSIONS

A joint NASA/Army/Bell Helicopter Textron wind-tunnel investigation was conducted in a preliminary assessment of the potential of generalized predictive control (GPC) for active stability augmentation in tiltrotor aircraft operating in the airplane mode of flight. The studies were made in the Langley Transonic Dynamics Tunnel using an unpowered 1/5-scale semispan aeroelastic model of the V-22 modified to incorporate an adaptive, GPC-based, MIMO active control algorithm to individually control the actuators of the fixed-system swashplate. Closed-loop stability of the model resulting from GPC inputs computed using feedback from wing-root strain gages was measured over a range of steady tunnel airspeeds for a single rotor rotational speed and two values of kinematic pitch-flap coupling. Performance of the system was also assessed in transient conditions by rapidly changing tunnel velocity and rotor speed about a nominal operating condition. Based on the results obtained in this investigation, the following conclusions are indicated:

1) The GPC algorithm employed was highly effective in increasing the stability (damping) in the critical wing mode of the model tested.

2) The GPC algorithm employed was also robust with respect to rapid changes in both the rotor speed and the airspeed, either singly or in combination.

3) All system identification and control law computations were done on-line, permitting rapid adaptation to changing conditions.

4) The swashplate angles required were modest, generally less than 0.3 degrees.

These results, in combination with equally successful results obtained in an earlier ground resonance test, suggest that a GPC-based active control system is a viable candidate for stability augmentation in advanced tiltrotor systems. Additional wind-tunnel tests of the WRATS model are planned to evaluate the GPC methodology over a broader range of operating conditions for the baseline stiff-inplane gimbaled rotor, as well as an advanced soft-inplane design.

REFERENCES

1. Hall, W. E.: Prop-Rotor Stability at High Advance Ratios. *Journal of the American Helicopter Society*, June 1966, pp. 11-26.

2. Edenborough, H. K.: Investigation of Tilt-Rotor VTOL Aircraft Rotor-Pylon Stability. *Journal of Aircraft*, Vol. 5, No. 6, March-April 1968, pp. 97-105.

3. Gaffey, T. M.; Yen, J. G.; and Kvaternik, R. G.: Analysis and Model Tests of the Proprotor Dynamics of a Tilt-Proprotor VTOL Aircraft. *Air Force V/STOL Technology and Planning Conference*, Las Vegas, NV, September 23-25, 1969.

4. Kvaternik, R. G.: *Studies in Tilt-Rotor VTOL Aircraft Aeroelasticity*. Ph.D. Dissertation, Case Western Reserve University, June 1973.

5. Johnson, W.: *Dynamics of Tilting Proprotor Aircraft in Cruise Flight*. NASA TN D-7677, May 1974.

6. Alexander, H. R.; Amos, A. K.; Tarzanin, F. J.; and Taylor, R. B.: *V/STOL Dynamics and Aeroelastic Rotor-Airframe Technology. Volume II: Description and Correlation of New Methodologies.* AFFDL-TR-72-40 (Volume II), September 1972.

7. Popelka, D.; Lindsay, D.; Parham, T.; Berry, V.; and Baker, D.: Results of an Aeroelastic Tailoring Study for a Composite Tiltrotor Wing. *American Helicopter Society 51st Annual Forum*, Forth Worth, TX, May 9-11, 1995.

8. Corso, L. M.; Popelka, D. A.; and Nixon, M. W.: Design, Analysis, and Test of a Composite Tailored Tiltrotor Wing. *American Helicopter Society 53rd An-*

nual Forum, Virginia Beach, VA, April 29 - May 1, 1997.

9. Nixon, M. W.; Piatak, D. J.; Corso, L. M.; and Popelka, D. A.: Aeroelastic Tailoring for Stability Augmentation and Performance Enhancements of Tiltrotor Aircraft. *American Helicopter Society 55th Annual National Forum*, Montreal, Canada, May 25-27, 1999.

10. Barkai, S. M; and Rand, O.: The Influence of Composite Induced Couplings on Tiltrotor Whirl Flutter Stability. *Journal of the American Helicopter Society*, Volume 43, No. 2, April 1998, pp. 133-145.

11. Srinivas, V.; Chopra, I.; and Nixon, M. W.: Aeroelastic Analysis of Advanced Geometry Tiltrotor Aircraft. *Journal of the American Helicopter Society*, Vol. 43, No. 3, July 1998, pp. 212-221.

12. Acree, C. W., Jr.; Peyran, R. J.; and Johnson, W.: Rotor Design for Whirl Flutter: An Examination of Options for Improving Tiltrotor Aeroelastic Stability Margins. *American Helicopter Society 55th Annual Forum*, Montreal, Quebec, Canada, May 25-27, 1999.

13. Alexander, H. R.; Eason, W.; Gillmore, K.; Morris, J.; and Spittle, R.: *V/STOL Tilt Rotor Aircraft Study. Volume 7: Tilt Rotor Flight Control Program Feedback Studies*. NASA CR-114600, March 1973.

14. Nasu, K.: *Tilt-Rotor Flutter Control in Cruise Flight*. NASA TM 88315, December 1986.

15. Van Aken, J. M.: Alleviation of Whirl-Flutter on Tilt-Rotor Aircraft Using Active Control. *American Helicopter Society 47th Annual Forum*, Phoenix, AZ, May 6-8, 1991, pp. 1321-1344.

16. Vorwald, J. G.; and Chopra, I.: Stabilizing Pylon Whirl Flutter on a Tilt-Rotor Aircraft. *32nd AIAA/ASME/ASCE/AHS/ASC Structures, Structural Dynamics, and Materials Conference*, Baltimore, MD, April 8-10, 1991 (Paper AIAA-91-1259-CP).

17. Clarke, D. W.; Mohtadi, C.; and Tuffs, P. S.: Generalized Predictive Control – Parts I and II. *Automatica*, Vol. 23, No. 2, 1987, pp. 137-160.

18. Kvaternik, R. G.; Juang, J.; and Bennett, R. L.: Exploratory Studies in Generalized Predictive Control for Active Aeroelastic Control of Tiltrotor Aircraft. *American Helicopter Society Northeast Region Specialists' Meeting on Active Controls Technology*, Bridgeport, CT, October 4-5, 2000 (Paper is also available as NASA/TM-2000-210552).

19. Richalet, J.; Rault, A.; Testud, J. L.; and Papon, J.: Model Predictive Heuristic Control: Applications to Industrial Processes. *Automatica*, Vol. 14, 1978, pp. 413-428.

20. Clark, D. W. (Ed): *Advances in Model-Based Predictive Control*. Oxford University Press, New York, 1994.

21. Juang, J.-N., *Applied System Identification*, Prentice Hall, Inc., Englewood Cliffs, New Jersey, 1994.

22. Eure, K.W.; and Juang, J.-N.: *Broadband Noise Control Using Predictive Techniques*. NASA TM 110320, January 1997.

23. Juang, J.-N.: *State-Space System Realization With Input- and Output-Data Correlation*. NASA TP 3622, April 1997.

24. Juang, J.-N.; and Phan, M. Q.: *Recursive Deadbeat Controller Design*. NASA TM 112863, May 1997 (also, *Journal of Guidance, Control, and Dynamics*, Vol. 21, No. 5, Sept.-Oct. 1998, pp. 747-753).

25. Juang, J.-N.; and Phan, M. Q.: *Deadbeat Predictive Controllers*. NASA TM 112862, May 1997.

26. Eure, K. W.: *Adaptive Predictive Feedback Techniques for Vibration Control*. Ph.D. Dissertation, Virginia Polytechnic Institute and State University, May 1998.

27. Phan, M. Q.; and Juang, J.-N.: Predictive Controllers for Feedback Stabilization. *Journal of Guidance, Control, and Dynamics*, Vol. 21, No. 5, Sept.-Oct. 1998, pp. 747-753.

28. Juang, J.-N.; and Eure, K. W.: *Predictive Feedback and Feedforward Control for Systems with Unknown Disturbances*. NASA/TM-1998-208744, December 1998.

29. Phan, M. Q.; and Juang, J-N: Predictive Feedback Controllers for Stabilization of Linear Multivariable Systems. *AIAA Guidance, Navigation and Control Conference*, San Diego, CA, July 29-31, 1996.

30. Settle, T. B.; and Kidd, D. L.: Evolution and Test History of the V-22 0.2-Scale Aeroelastic Model. *Journal of the American Helicopter Society*, Vol. 37, No. 1, January 1992, pp. 31-45.